

Journal of Thermal Engineering

Web page info: https://jten.yildiz.edu.tr DOI: 10.14744/thermal.0001031



Research Article

Study the influence of thermophoretic effect buoyancy force in prandtl fluid flow on a stretching sheet in presence of joule heating and viscous dissipation

Puspanjali MAHAPATRA^{1,2}, Tusar Kumar PARIDA³, Kharabela SWAIN^{4,*}

¹Department of Mathematics, Silicon University, Bhubaneswar, 751024, India ²Department of Mathematics, Dhenkanal Autonomous College, Dhenkanal, 759001, India ³Department of Mathematics, Silicon Unversity, Bhubaneswar, 751024, India ⁴Department of Mathematics, GIFT Autonomous, Bhubaneswar, 752054, India

ARTICLE INFO

Article history
Received: 30 September 2024
Revised: 6 June 2025
Accepted: 13 March 2025

Keywords:

Brownian Motion; Buoyancy Force; Chemical Reaction; Joule Heating; Prandtl Fluid; Stretching Sheet; Thermophoresis; Viscous Dissipation

ABSTRACT

There are many natural phenomena and engineering usage susceptible to magneto fluid dynamics. The boundary layer theory is precisely such as asymptotic theory for the ease of very large Reynolds number. A numerical investigation was made to analyze the effects of Brownian motion, thermophoresis, and buoyancy force of non-Newtonian nanofluid relying on the Prandtl fluid model over a stretching sheet. The energy equation is empowered by the influence of Joule heating, viscous dissipation, and thermal radiation, whereas the concentration equation is determined by a chemical reaction. Similarity transformations are used to convert the governing partial differential equations (PDEs) into a system of nonlinear ordinary differential equations (ODEs). The resulting systems are effectively solved using the numerical scheme known as the Runge-Kutta-Fehlberg's method with shooting technique and bvp4c solver in MATLAB code. The graphical results show the effect of pertinent parameters under buoyancy-assisting/opposing forces on velocity, temperature, and concentration profiles. Momentum transport gets accelerated for higher material/characteristic parameter of the non-Newtonian fluid model irrespective of presence or absence of porous matrix but thermal energy gets depleted for higher material parameter across the flow domain contributing to thermal stability. The elastic property of the Prandtl fluid and the effect of electromagnetic force increase slightly the solutal concentration but significantly to temperature. Thus, it is concluded that the generated Lorentz force (the additional body force) increases the thermal transport and solutal concentration of non-Newtonian nanofluid model.

Cite this article as: Mahapatra P, Parida TK, Swain K. Study the influence of thermophoretic effect buoyancy force in prandtl fluid flow on a stretching sheet in presence of joule heating and viscous dissipation. J Ther Eng 2025;11(6):1647–1657.

This paper was recommended for publication in revised form by Editor-in-Chief Ahmet Selim Dalkilic



^{*}Corresponding author.

^{*}E-mail address: kharabela1983@gmail.com

INTRODUCTION

Generally, metallic oxides, metals, or carbon nanotubes nanoparticles etc are mixed with a base fluid, like ethylene glycol, water, or oil, to produce nanofluid. They exhibit an improved thermal, optical, and electrical properties. Choi [1] initially proposed the idea of a nanofluid, demonstrating how adding nanoparticles to a fluid can dramatically increase its thermal conductivity. The boundary layer flow, past a stretched plate in a viscous fluid, is studied by Siddappa and Abel [2]. The heat transmission across a stretched sheet with varying wall temperature and internal heat generation of an electrically conducting fluid are examined by Vajravelu et al. [3]. Wang et al. [4] focused on the fluid flow and heat transmission properties of nanofluids in both forced and free convection flows. The inadequacy of macroscopic analysis on heat transfer in nanofluids is examined by Keblinski et al. [5]. They also provide explanations with experiments for the fluids with higher thermal conductivity. Furthermore, a number of researchers [6-10] investigated the different aspects of viscous nanofluid flows across a stretching surface due to their distinct and durable qualities. The nanofluids applications in a variety of industries, including manufacturing, microelectronics, thermal power, and biomedicines.

Non-Newtonian fluids are used in many technological processes as well as house hold usage including toothpaste, paints, emulsions, oil, and polymer sheets. The class of non-Newtonian fluids is divided into many branches. The shear thinning fluid is one of the most significant branch. In these fluids, the apparent viscosity decreases with applied shear force. Many fluid models are proposed to explain the characteristics of shear thinning fluids. The Prandtl fluid model is one which can adequately explain the shear thinning phenomenon. Kuik [11] worked on Prandtl's solution on examining the flow at infinity. The flow around an exponential spiral with a finite length, is first studied in order to introduce a length scale. Prandtlys equations are recovered in the limit for infinite spiral length. Khan et al. [12] discovered the effects of homogenous/ heterogeneous reactions on 2-D flow of Prandtl fluid over a stretching sheet. Ganesh Kumar et al. [13] considered Joule heating, to study the melting effects, on flow of Prandtl fluid over an expanded sheet and found that velocity profiles are directly proportional to the Prandtl parameter. Eid et al. [14] studied the 3-D flow and heat transfer of Prandtl nanofluid over a convectively heated porous sheet in the presence of non-linear radiation and higher order chemical reaction. Asad [15] examined entropy generation on the mixed convective MHD flow of Prandtl fluid past a non-linear stretched sheet. Zafar et al. [16] investigated the irreversibility flow of Prandtl nanofluid over a stretched surface in Darcy-Forchheimer medium.

The buoyant force produced by temperature changes within a flow domain is referred to as thermal buoyancy. The interplay of heat and mass transfer along with buoyancy effects is crucial in a wide range of practical applications to enhance the efficiency and effectiveness of various thermal and chemical processes like solar collectors, nuclear reactor coolants, chemical process industries, environmental engineering, etc. Raju and Sandeep [17] considered the assisting/opposing flow of non-Newtonian fluid past a cone with Lorentz force. Habib et al. [18] studied the importance of Stephen blowing and Lorentz force on dynamics of Prandtl nanofluid using Keller box method. Further, Yaseen et al. [19] considered hybrid nanofluid flow past a permeable moving surface. Ramanjini et al. [20] examined the effects of first-order slip, and chemical reaction on unsteady Prandtl nanofluid flow through stretching sheet due to mixed convection. Recently, many researchers [21-33] explained the importance of flow of nanofluid and hybrid nanofluid using different flow geometry.

The following salient features are embodied in the present analysis:

- Impacts of Joule heating, thermal radiation, chemical reaction, and viscous dissipation on the flow.
- The contributions of thermophoresis and Brownian motion on the heat transfer.
- Buoyancy assisting/opposing flow of nanofluid.
- The solution of mathematical model by Runge-Kutta-Fehlberg's scheme with bvp4c solver in MATLAB code.

Research Questions

The following scientific research issues are addressed in this study:

- The effects of Lorentz force, fluid parameter, elastic parameter and porosity parameter on the velocity profile.
- The transport of heat in presence of Joule heating, viscous dissipation and Brownian motion.
- The effect of chemical reaction parameter, Schmidt number, thermophoresis, and Brownian motion on nanoparticle concentration.
- Variations of skin friction coefficient, Nusselt number, and Sherwood number, the surface criteria, due to change in fluid parameter, elastic parameter, Eckert number and Biot number.

Mathematical Formulation

Consider a two-dimensional, steady and incompressible flow of nanofluid on a stretching sheet as illustrated in Figure 1. Impacts of thermophoresis and Brownian motion on the flow are taken into account. Further, Joule heating, thermal radiation and viscous dissipation empower the energy equation. The x-axis is taken along the stretching sheet and the y-axis is vertical to the flow direction. The sheet is stretched with the velocity $u_w(x) = ax$ with a > 0, a constant. The temperature and concentration of the stretching surface are taken as T_w , and C_w while the ambient temperature and concentration are at T_∞ and C_∞ .

The following assumptions are made:

- The nanofluid is considered to be non-Newtonian and incompressible.
- Both the nanoparticles and fluid phase are in thermal equilibrium.
- The induced magnetic field is so small (low magnetic Reynolds number) and hence it is ignored.
- The constant uniform transverse magnetic field of strength B₀ is applied to the sheet.

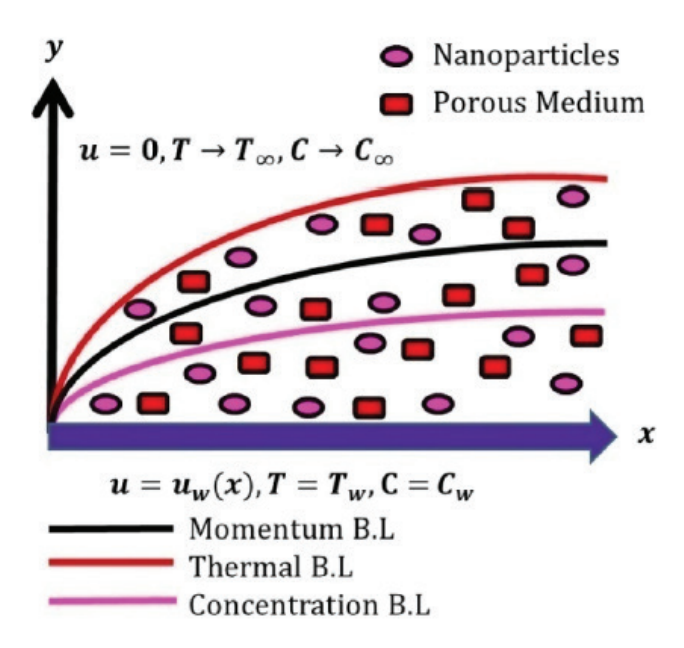


Figure 1. Physical model of the problem.

The Cauchy stress tensor for the Prandtl fluid is given by

$$S = \frac{A \sin^{-1} \left\{ \frac{1}{c_1} \left[\left(\frac{\partial u_i}{\partial x_j} \right)^2 + \left(\frac{\partial u_j}{\partial x_i} \right)^2 \right]^{\frac{1}{2}} \right\}}{\left[\left(\frac{\partial u_i}{\partial x_j} \right)^2 + \left(\frac{\partial u_j}{\partial x_i} \right)^2 \right]^{\frac{1}{2}}} A_1$$
 (1)

where A and c_1 are the material parameters and A_1 is the first Rivlin-Erickson tensor.

Under the above assumptions, the governing equations and corresponding boundary conditions are given by [15, 20]

$$\frac{\partial u}{\partial x} + \frac{\partial v}{\partial y} = 0,\tag{2}$$

$$u\frac{\partial u}{\partial x} + v\frac{\partial u}{\partial y} = v\frac{A}{c_1} \left\{ 1 + \frac{1}{2c_1^2} \left(\frac{\partial u}{\partial y} \right)^2 \right\} \frac{\partial^2 u}{\partial y^2} - \frac{\sigma B_0^2}{\rho} u$$

$$-\frac{v}{k^*} u + g\beta_1 \left(T - T_\infty \right), \tag{3}$$

$$u\frac{\partial T}{\partial x} + v\frac{\partial T}{\partial y} = \left(\zeta + \frac{16\sigma^* T_{\infty}^3}{3\rho c_p k^*}\right)\frac{\partial^2 T}{\partial y^2} + \frac{\sigma B_0}{\rho c_p} u^2 + \frac{\left(\rho c\right)_p}{\left(\rho c\right)_f} \left\{D_B \frac{\partial C}{\partial y} \frac{\partial T}{\partial y} + \frac{D_T}{T_{\infty}} \left(\frac{\partial T}{\partial y}\right)^2\right\} + \frac{\mu}{\rho c_p} \left(\frac{\partial u}{\partial y}\right)^2, \tag{4}$$

$$u\frac{\partial C}{\partial x} + v\frac{\partial C}{\partial y} = D_B \frac{\partial^2 C}{\partial y^2} + \frac{D_T}{T_\infty} \frac{\partial^2 T}{\partial y^2} - k_c \left(C - C_\infty\right). \tag{5}$$

Boundary conditions

$$at y = 0: u = ax, v=0, -k \frac{\partial T}{\partial y} = h(T_w - T), C=C_w,$$

$$as y \to \infty: u \to 0, T \to T_\infty, C \to C_\infty.$$
(6)

Similarity transformations

The boundary layer equations (2) - (5) admit of a similarity solutions

$$u = axf'(\eta), v = -\sqrt{av}f, \theta(\eta) = \frac{T - T_{\infty}}{T_{w} - T_{\infty}},$$

$$\phi(\eta) = \frac{C - C_{\infty}}{C_{w} - C_{\infty}}.$$
(7)

where $\eta = \sqrt{\frac{a}{v}}y$ is the non-dimensional vertical distance measured from the surface of the stretching sheet.

Now the equations (2) – (6) become

$$\alpha \left(1 + \beta f^{\dagger \prime \prime 2}\right) f^{\dagger \prime \prime \prime} + f f^{\prime \prime \prime} - f^{\prime 2} - M f^{\prime \prime} - k_p f^{\prime \prime} + \lambda \theta = 0 \quad (8)$$

where $f'(\eta)$ and $f(\eta)$ represent horizontal and vertical velocity components respectively.

$$\frac{1}{\mathbf{Pr}} \left(1 + \frac{4}{3} R \right) \theta'' + f \theta' + Nb\theta' \phi' + Nt\theta'^{2}$$

$$-MEcf'^{2} + Ecf''^{2} = 0$$
(9)

$$\phi'' + \frac{Nt}{Nb}\theta'' + Scf\phi' - k_{r}Sc\phi = 0$$
 (10)

$$(2) \qquad f(0) = 0, f'(0) = 1, \theta'(0) = -\gamma \left[1 - \theta(0)\right], \phi(0) = 1,$$

$$f'(\infty) = 0, \theta(\infty) = 0, \phi(\infty) = 0.$$

$$(11)$$

M	Hibab et al. [18]	Ramanjini et al. [20]	Present study
0	-1.8428	-1.8478	-1.8465
1	-1.0100	-1.0012	-1.0126
5	-0.5213	-0.5205	-0.5218
10	-0.4150	-0.4156	-0.4162

Table 1. Comparison of skin friction coefficient f''(0) for different values of M

Physical parameters of engineering interest

The physical parameters such as the skin friction coefficient, local Nusselt number, and local Sherwood number are respectively defined as

$$C_f = \frac{2\tau_w}{\rho u_w^2}, Nu_x = \frac{xq_w}{k(T_w - T_\infty)}, \text{ and } Sh_x = \frac{xq_m}{D_B(C_w - C_\infty)}$$
 (12)

Here,
$$\tau_w = \mu \left(\frac{\partial u}{\partial y}\right)_{y=0}$$
 (shear stress),
$$q_w = -k \left(\frac{\partial T}{\partial y}\right)_{y=0} + \left(q_r\right)_{y=0}$$
 (heat flux), and
$$q_m = -D_B \left(\frac{\partial C}{\partial y}\right)_{y=0}$$
 (mass flux).

Finally, we get
$$\sqrt{\operatorname{Re}_{x}}C_{f} = f''(0)$$
,
$$\sqrt{\operatorname{Re}_{x}}Nu_{x} = -\left(1 + \frac{4}{3}R\right)\theta'(0), \sqrt{\operatorname{Re}_{x}}Sh_{x} = -\phi'(0)$$
 (13)

Work Validation

The system of non-linear coupled ODEs with prescribed boundary conditions (8-11) are solved numerically by Runge-Kutta Fehlberg's method combined with Shooting technique using bvp4c solver in MATLAB code. The convergence, stability and accuracy of the method has been carried out with step size 10^{-2} and error tolerance 10^{-5} . The computation of the skin friction coefficient has been made when ($\alpha = \beta = 0.2$, Pr = 1, $Ec = k_p = Sc = k_r = Nt = 0$, $Nb \rightarrow 0$ for various values of M which are shown in Table 1. These outcomes are found in good agreement with the results reported by Hibab et al. [18] and Ramanjini et al. [20].

In this method, the governing equations are reduced to a set of following first order differential equations.

$$\begin{split} f_{1}^{'} &= f_{2} \\ f_{2}^{'} &= f_{3} \\ f_{3}^{'} &= -\left(\frac{1}{\alpha \left(1 + \beta f_{3}^{2}\right)}\right) \left[f_{1}f_{3} - f_{2}^{2} - \left(M + k_{p}\right)f_{2} + \lambda \theta\right] \end{split}$$

$$\begin{aligned} \theta_{1}^{'} &= \theta_{2} \\ \theta_{2}^{'} &= -\frac{\Pr}{\left(1 + \frac{4}{3}R\right)} \left(f_{1}\theta_{2} + Nb\theta_{2}\phi_{2} + Nt\theta_{2}^{2} - MEcf_{2} + Ecf_{3}^{2}\right) \end{aligned}$$

$$\begin{split} \phi_{1}^{'} &= \phi_{2} \\ \phi_{2}^{'} &= -\left[\frac{Nt}{Nb}\theta_{2} + Sc\left\{f_{1}\phi_{2} - k_{r}\phi_{1}\right\}\right] \end{split}$$

subject to the initial conditions

$$f_{1}(0) = 0, f_{2}(0) = 1, \theta_{1}(0) = -\gamma \left[1 - \theta_{1}(0)\right], \phi_{1}(0) = 1$$

$$f_{3}(0) = r_{1}, \theta_{2}(0) = r_{2}, \phi_{2}(0) = r_{3}$$

where r_1 , r_2 and r_3 are are guess values to be prescribed during computation. A self-corrective procedure has been applied to improve the accuracy.

RESULTS AND DISCUSSION

Figure 2 depicts the effect of material parameter (α) and porosity parameter (k_p) on the horizontal component of velocity distribution in the boundary layer, the domain of interest. The velocity decreases asymptotically to attain its ambient state throughout the flow field. Moreover, it increases with an increase in the value of Prandtl fluid parameter (α) . It is interesting to note that when $\alpha=0$, equation (8), the momentum transport equation, reduces to an electrically conducting Newtonian fluid with a transverse magnetic field and the order of differential equation is reduced by 1 i.e. from third order to second order which is the usual characteristics of non-Newtonian fluid. Further, it is seen that fluid velocity decreases in the presence of porous medium $(k_p=0.5)$, due to constricted passage and resistivity of porosity term which appears with a negative sign.

Figure 3 shows a fall in temperature distribution asymptotically for higher values of non-Newtonian/material parameter. Thus, it is concluded that the present non-Newtonian fluid model reduces the thermal power in the boundary layer for higher values of characteristic parameter irrespective of porosity of the medium. This is an important observation pertaining to the present fluid model. This may

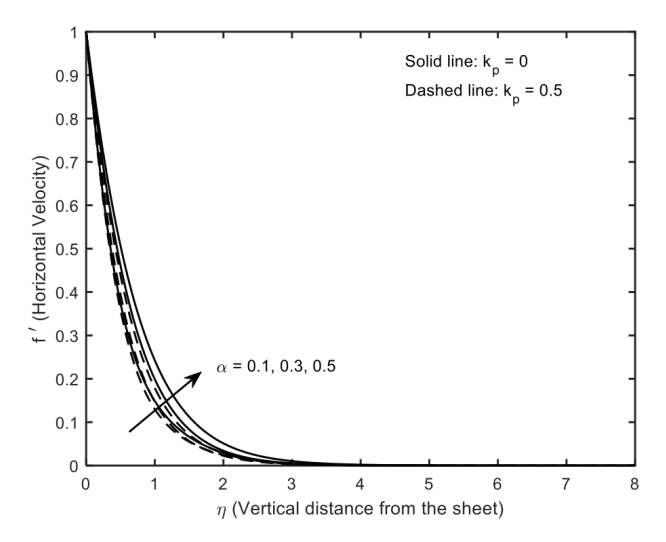


Figure 2. Impact of α and k_p on $f'(\eta)$.

be of industrial use when asymptotic fall in thermal energy level is required for higher value of material parameter that is mostly required for thermal stability of the flow. From Figure 4 it is seen that the nanoparticle solutal concentration distribution decreases layer wise as well as vertically same as that of temperature distribution.

Figures. 5 and 6 show the fall of concentration and temperature across the flow field for higher elasticity fluid property. The effect of higher magnetic field intensity results in strengthen of both temperature and concentration level but the higher magnetic field intensity rises slightly concentration (Fig. 5) and significantly temperature distribution (Fig. 6). It is concluded that electromagnetic force affects significantly thermal property of the fluid but not to nanoparticle concentration.

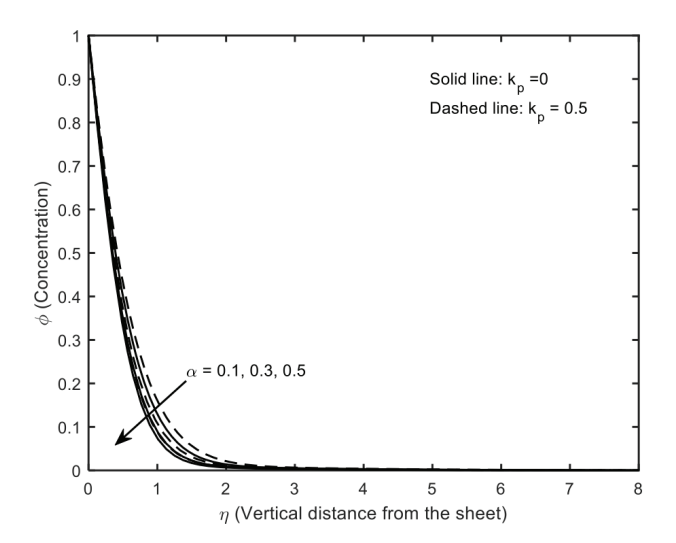


Figure 4. Impact of α and k_p on $\phi(\eta)$.

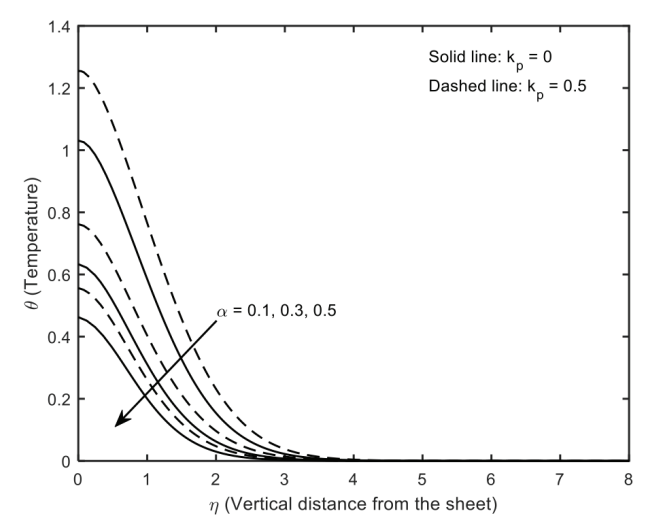


Figure 3. Impact of α and k_p on $\theta(\eta)$.

Figure 7 depicts that an increase in elastic property of the fluid as well as electromagnetic body force. Higher magnetic field strength increases the velocity but opposite effect is observed in case of elastic parameter. This outcome finds application in an appropriate field of interest such as chemical processing unit where reducing the velocity distribution is essential by regulating voltage vis-à-vis magnetic field strength in an electric circuit and thermal power system.

Figure 8 depicts the effect of two important parameters namely thermal buoyancy and Biot number on solutal concentration. It is observed that an increase in thermal buoyancy decreases the solutal concentration but the reverse effect is observed in case of Biot number. As the thermal buoyancy assisting parameter $\lambda > 0$ increases that leads

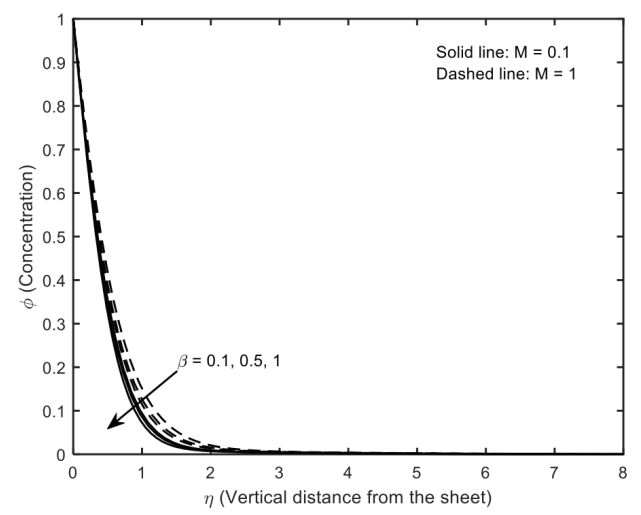
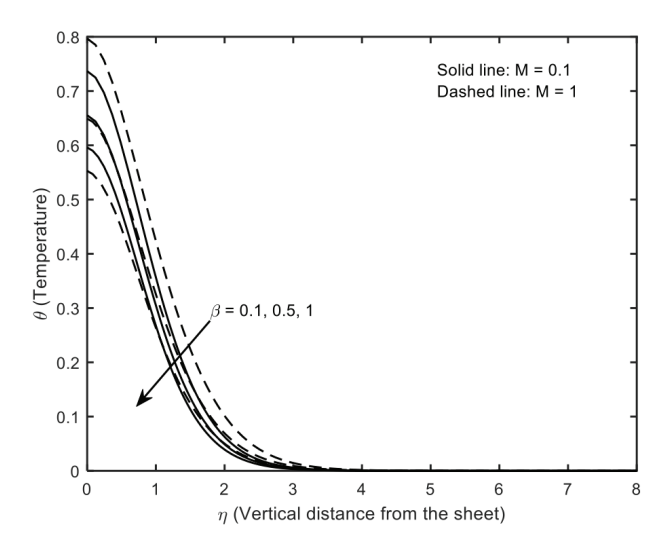


Figure 5. Impact of β and M on $\phi(\eta)$.



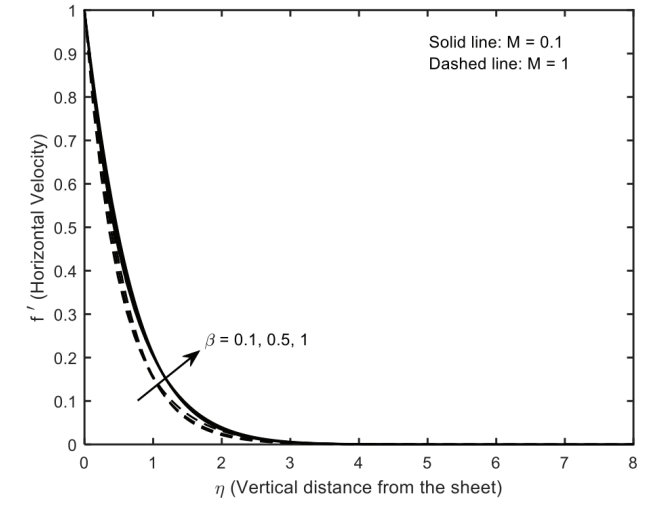


Figure 6. Impact of β and M on $\theta(\eta)$.

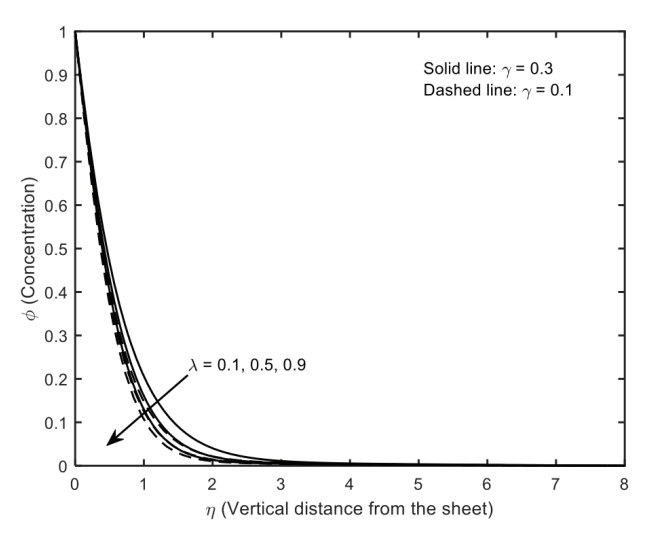
Figure 7. Impact of β and M on $f'(\eta)$.

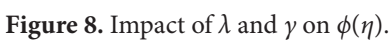
to decrease the solutal concentration but in case of Biot number the solutal concentration increases. The results admit of a physical interpretation as: since $\gamma > 0$ relates to Newtonian cooling and Biot number being an index of the ratio of the heat transfer resistances inside the flow domain to that of bounding surface, the concentration increases in the flow domain.

Figure 9 shows that the temperature distribution admits of the same effect as that of concentration for both the parameters. The explanation is provided in case of Figure 8. Thus, higher Biot number enhances the fluid temperature resulting cooling of the bounding surface. It serves as a cooling device of the stretching surface resulting a desired quality product specifically in polymer processing. On careful observation of Figures. 8 and 9 it is remarked that in case of buoyancy assisting flow, the

volume fraction of nanoparticle i.e. concentration behave in same way as that of temperature variation in case of enhanced thermal buoyancy parameter (λ) i.e. down grading the concentration and temperature due to enhanced thermal buoyancy.

Figure 10 depicts a higher velocity distribution with $\lambda > 0$ i.e. in case of buoyancy assisting flow the velocity increases. The result coincides with physics of the buoyant force. The Biot number (γ) also enhances the fluid velocity but slightly. Figures. 11 and 12 show the effect of thermophoresis (Nt) and Brownian diffusion (Nb) on concentration and temperature distributions respectively. The higher thermophoresis enhances the solutal concentration but higher Brownian diffusion downgrades the level of concentration in the flow domain. The physical





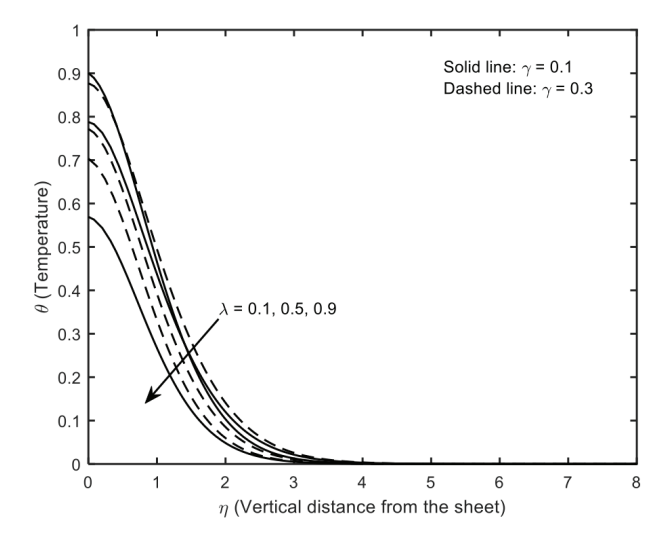
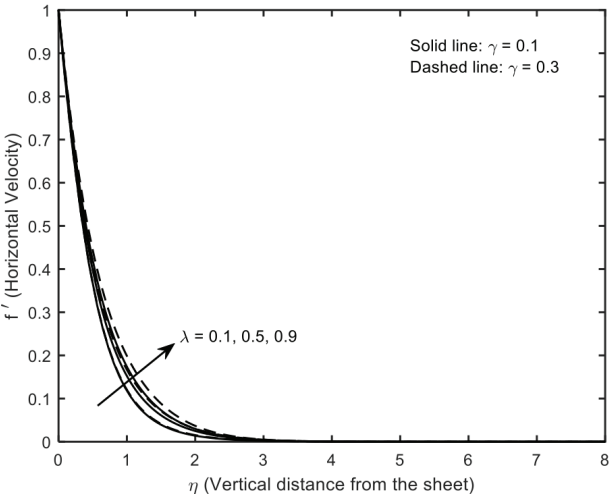


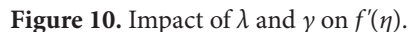
Figure 9. Impact of λ and γ on $\theta(\eta)$.

Solid line: Nb = 0.5

5

Dashed line: Nb = 0.1



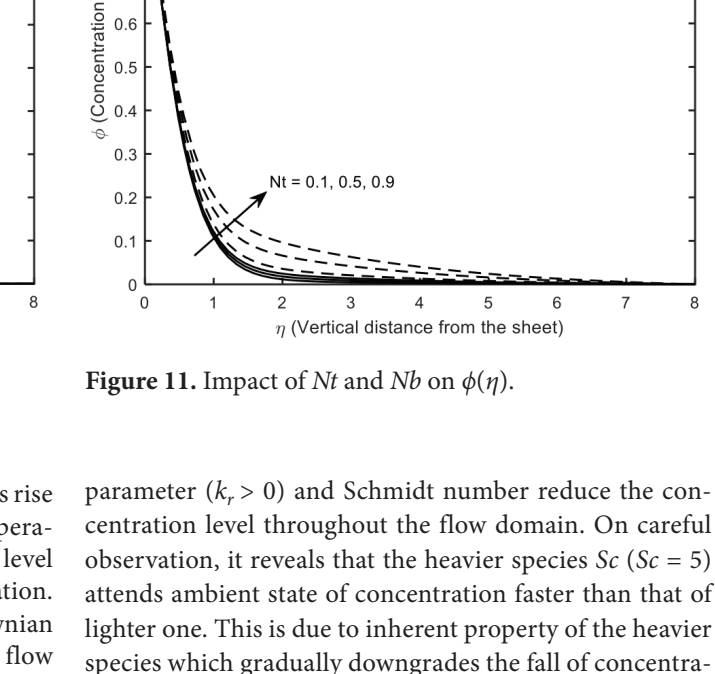


reasoning attributed as follows: thermo diffusion gives rise to the additional mass transfer because of the temperature gradient contributing to higher concentration level but Brownian motion reduces the level of concentration. Figure 12 shows that both thermophoresis and Brownian motion enhance temperature distribution in the flow domain. Figure 13 presents the effects of two important parameters such as *Ec* and *R* on temperature distribution. It is interesting to note that both the parameters enhance the temperature distribution. The Eckert number is a measure of the dissipation effects in the flow. Since this grows in proportion to the square of velocity, it can be neglected for small velocity. The observed finding is that tempera-

ture increases with higher values of Ec as well as radiation

parameter (R). The effect of Ec is more distinct. Figure 14

depicts that enhancement of destructive chemical reaction



0.9

0.8

0.7

0.6

tion level to reach ambient state. The values of skin friction coefficient, Nusselt number and Sherwood number is computed and shown in Table 2. It is seen that fluid parameter, elastic parameter and thermal buoyancy parameter increases the magnitude of $-\theta'(0)$, f''(0) and $-\phi'(0)$ whereas Brownian motion have same effect on $-\theta'(0)$ but opposite effect s observed in case of $-\phi'(0)$. Further, destructive and constructive chemical reaction

have opposite effects on Sherwood number.

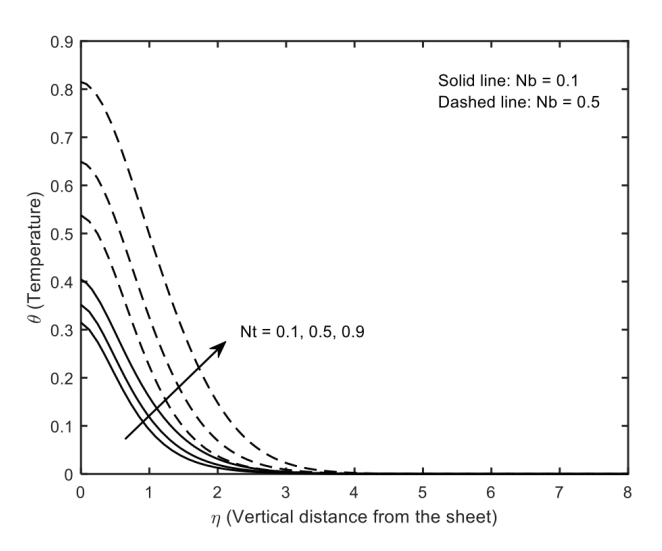


Figure 12. Impact of *Nt* and *Nb* on $\theta(\eta)$.

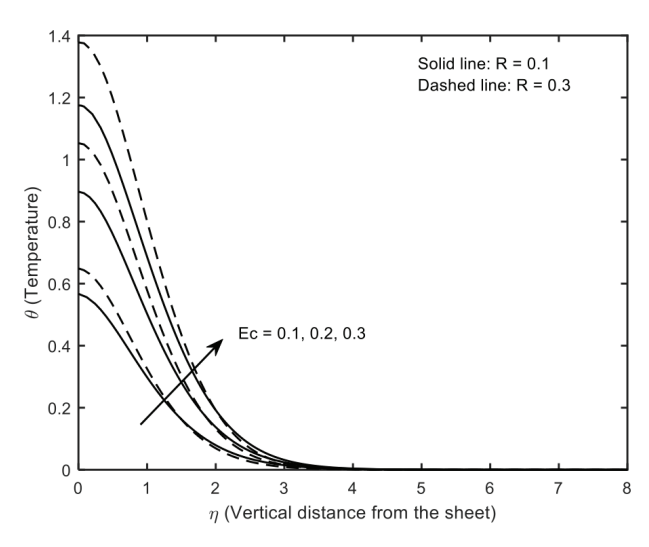


Figure 13. Impact of *Ec* and *R* on $\theta(\eta)$.

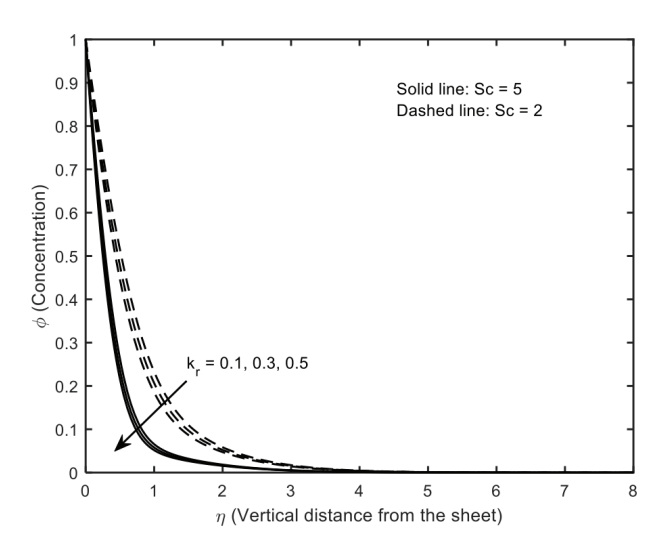


Figure 14. Impact of k_r and Sc on $\phi(\eta)$.

CONCLUSION

From the present study, the following conclusions can be drawn:

- Momentum transport gets accelerated for higher material/characteristic parameter of the non-Newtonian fluid model irrespective of presence or absence of porous matrix (Fig. 2) but thermal energy gets depleted for higher material parameter across the flow domain contributing to thermal stability (Fig. 3).
- The nanoparticle solutal concentration distribution decreases layer wise as well as vertically same as that of temperature distribution (Fig. 4). The elastic property of the Prandtl fluid and the effect of electromagnetic force increase slightly the solutal concentration but significantly to temperature. Thus, it is concluded that the generated Lorentz force (the additional body force)

Table 2. Computation of f''(0), $-\theta'(0)$ and $-\phi'(0)$ when $M = k_p = 1.0$, Pr = 0.71, Sc = 0.6.

α	β	λ	Nb	Nt	Ec	λ	k_r	<i>f</i> "(0)	- heta'(0)	$-\phi'(0)$
0.1	0.1	0.1	0.1	0.1	0.1	0.1	0.1	-0.809671	0.093315	0.966063
0.3								-0.568545	0.099859	1.023789
0.5								-0.451017	0.102874	1.051753
	0.3							-0.449584	0.102895	1.052040
	0.5							-0.448189	0.102917	1.052321
	1.0							-0.444854	0.102968	1.052998
		0.3						-0.432493	0.103034	1.054064
		0.5						-0.420224	0.103098	1.055120
		1.0						-0.389938	0.103250	1.057718
			0.2					-0.382747	0.102342	1.085527
			0.3					-0.374647	0.101338	1.095509
			0.5					-0.355330	0.099006	1.105087
				0.2				-0.354459	0.098913	1.097858
				0.5				-0.351742	0.098624	1.076792
				0.9				-0.347859	0.098217	1.050225
					0.2			-0.366950	0.101039	1.029284
					0.3			-0.384687	0.103674	1.009820
					0.5			-0.413456	0.104713	0.980635
						0.2		-0.327032	0.190967	0.932763
						0.3		-0.246689	0.244508	0.911678
						0.5		-0.118833	0.339039	0.880934
							0.3	-0.414595	0.108160	1.145392
							0.5	-0.412800	0.107910	1.297682
							-0.1	-0.419115	0.108788	0.778311
							-0.3	-0.422152	0.109213	0.540814
							-0.5	-0.426185	0.109763	0.227303

increases the thermal transport and solutal concentration of non-Newtonian nanofluid model.

- Biot number being the index of the heat transfer resistance that enhances the concentration level of the nanoparticle.
- The higher thermophoresis enhances the concentration level that is an asset for the quality product.
- The Eckert number being the measure of dissipative effects that enhance the temperature distribution co-opted with radiation effect.
- The heavier species contribute to lower level of concentration which may be of industrial use with a care to destructive reaction rate as it is detrimental to level of concentration.

σ^*	Stefan-Boltzmann constant
μ	Coefficient of viscosity
a	Constant
k^*	Coefficient of absorption
g	Gravitational force due to
	gravity
σ	Electrical conductivity
T	Fluid temperature
T_{∞}	Ambient temperature
C	Nanoparticle concentration
C_{∞}	Ambient concentration
f	Dimensionless velocity
θ	Dimensionless temperature
ϕ	Dimensionless concentration

ABBREVIATIONS

7.551.51.51.61.6	
$\alpha = \frac{A}{c_1}$	Material parameter
$\beta = \frac{a^2 \operatorname{Re}_x}{2c_1^2}$	Elastic parameter
$\gamma = \frac{h}{k} \sqrt{\frac{\nu}{a}}$	Biot number
$M = \frac{\sigma B_0^2}{a\rho}$	Magnetic parameter
$k_p = \frac{ak^*}{v}$	Porosity parameter
$\lambda = \frac{g\beta}{a^2x} \left(T_w - T_\infty \right)$	Thermal buoyancy parameter
$R = \frac{4\sigma^* T_{\infty}^3}{kk^*}$	Radiation parameter
$\Pr = \frac{v}{\zeta}$	Prandtl number
$Nb = \frac{\left(\rho c\right)_{p} D_{B}}{\left(\rho c\right)_{f} \upsilon} \left(C_{w} - C_{\infty}\right)$	Brownian diffusion parameter
$Nt = \frac{\left(\rho c\right)_{p} D_{T}}{\left(\rho c\right)_{f} T_{\infty} \upsilon} \left(T_{w} - T_{\infty}\right)$	Thermophoresis parameter
$Ec = \frac{u_w^2}{c_p(T_w - T_\infty)}$	Eckert number
$Sc = \frac{\upsilon}{D_B}$	Schmidt number

Chemical reaction parameter

Local Reynolds number

Thermal diffusivity

Effective heat capacity

Heat capacity of fluid

Density of the fluid

Kinematic viscosity

AUTHORSHIP CONTRIBUTIONS

Authors equally contributed to this work.

DATA AVAILABILITY STATEMENT

The authors confirm that the data that supports the findings of this study are available within the article. Raw data that support the finding of this study are available from the corresponding author, upon reasonable request.

CONFLICT OF INTEREST

The author declared no potential conflicts of interest with respect to the research, authorship, and/or publication of this article.

ETHICS

There are no ethical issues with the publication of this manuscript.

STATEMENT ON THE USE OF ARTIFICIAL INTELLIGENCE

Artificial intelligence was not used in the preparation of the article

REFERENCES

- [1] Choi SUS. Enhancing thermal conductivity of fluids with nanoparticles: In: Developments and applications of non-Newtonian flows. ASME 1995;99–105.

 [Crossref]
- [2] Siddappa B, Abel S. Non-Newtonian flow past a stretching plate. Z Angew Math Phys 1985;36:890–892. [Crossref]
- [3] Vajravelu K, Rollins D. Heat transfer in an electrically conducting fluid over a stretching surface. Int J Non Linear Mech 1992;27:265–277. [Crossref]

- [4] Wang XQ, Mujumdar AS. Heat transfer characteristics of nanofluids: A review. Int J Therm Sci 2007;46:1–19. [Crossref]
- [5] Keblinski P, Phillpot SR, Choi SUS, Eastman JA. Mechanisms of heat flow in suspensions of nanosized particles (nanofluids). Int J Heat Mass Transf 2002;45:855–863. [Crossref]
- [6] Swain K, Mahanthesh B, Mebarek-Oudina F. Heat transport and stagnation-point flow of magnetized nanoliquid with variable thermal conductivity, Brownian moment, and thermophoresis aspects. Heat Transfer 2021;50:754–767. [Crossref]
- [7] Biswal MM, Swain K, Dash GC, Ojha KL. Study of radiative magneto-non-Newtonian fluid flow over a nonlinearly elongating sheet with Soret and Dufour effects. Numer Heat Transf A Appl 2023;83:331–342.

 [Crossref]
- [8] Ghennai A, Bessaïh R. Heat transfer enhancement in a cubical cavity filled with a hybrid nanofluid. Heat Transfer 2021;50:1658–1678. [Crossref]
- [9] Santosh C, Parida SK. Heat transfer analysis of MHD viscous nanofluid flow over a nonlinearly stretching sheet with heat source/sink: A numerical study. Numer Heat Transf A Appl 2023;1–20. [Crossref]
- [10] Jena S, Swain K, Ibrahim SM, Sreenivasulu P, Lorenzini G. Three-dimensional MHD rotating flow of radiative nanofluid over a stretched sheet with homogeneous-heterogeneous chemical reactions. J Eng Thermophys 33:336–353. [Crossref]
- [11] Kuik GAM van. The flow induced by Prandtl's self-similar vortex sheet spirals at infinite distance from the spiral kernel. Eur J Mech B Fluids 2004;23:607–616. [Crossref]
- [12] Khan I, Malik MY, Hussain A, Salahuddin T. Effect of homogeneous-heterogeneous reactions on MHD Prandtl fluid flow over a stretching sheet. Results Phys 2017;7:4226–4231. [Crossref]
- [13] Ganesh Kumar K, Krishnamurthy MR, Rudraswamy NG. Boundary layer flow and melting heat transfer of Prandtl fluid over a stretching surface by considering Joule heating effect. Multidiscip Model Mater Struct 2019;15:337–352.
- [14] Eid MR, Mabood F, Mahny KL. On 3D Prandtl nanofluid flow with higher-order chemical reaction. Proc Inst Mech Eng C J Mech Eng Sci 2021;235:3962–3974.
- [15] Asad S. Nonlinear stretched flow a radiative MHD Prandtl fluid with entropy generation and mixed convection. Front Phys 2023;11:1150457. [Crossref]
- [16] Zafar SS, Khan U, Ali F, Eldin SM, Mohammed Saeed A, Zaib A, Galal AM. Irreversibility analysis of radiative flow of Prandtl nanofluid over a stretched surface in Darcy–Forchheimer medium with activation energy and chemical reaction. Heliyon 2023;9:e14877. [Crossref]

- [17] Raju CSK, Sandeep N. Opposing and assisting flow characteristics of radiative Casson fluid due to cone in the presence of induced magnetic field. Int J Adv Sci Technol 2016;88:43–62. [Crossref]
- [18] Habib D, Salmat N, Hussain S, Ali B, Abdal S. Significance of Stephen blowing and Lorentz force on dynamics of Prandtl nanofluid via Keller box approach. Int Commun Heat Mass Transf 2021;128:105599. [Crossref]
- [19] Yaseen M, Manoj Kumar, Rawat SK. Assisting and opposing flow of a MHD hybrid nanofluid flow past a permeable moving surface with heat source/sink and thermal radiation. Partial Differ Equ Appl Math 2021;4:100168. [Crossref]
- [20] Ramanjini V, Gopi Krishna G, Ramanuja M, Sree HK, Mishra SR. Unsteady Prandtl nanofluidic flow through stretching sheet due to mixed convection, first-order slip, and chemical reaction. J Niger Soc Phys Sci 2023;5:1140. [Crossref]
- [21] Shaw S, Patra A, Misra A, Nayak MK. Assisting/opposing/forced convection flow on entropy-optimized MHD nanofluids with variable viscosity: Interfacial layer and shape effects. Heat Transfer 2022;51:578–603. [Crossref]
- [22] Kavya S, Nagendramma V. Opposing and assisting flow of a hybrid Newtonian/non-Newtonian nanofluid past a stretching cylinder. J Mines Met Fuels 2023;71:1045–1057.
- [23] Sinha S, Gupta P, Filippov AN. Buoyancy assisting and opposing mixed convective MHD flow of nanofluid along a vertical stretching sheet. Colloid J 2023;85:128–139. [Crossref]
- [24] Nagaraja KV, Khan U, Madhukesh JK, Ahmed M Hassan, Prasannakumara BC, Kahla NB, Elattar S, Chohan JS. Heat and mass transfer analysis of assisting and opposing radiative flow conveying ternary hybrid nanofluid over an exponentially stretching surface. Sci Rep 2023;13:14795. [Crossref]
- [25] Khan U, Zaib A, Ishak A, Sherif EM, Sarris IE, Eldin SM, Pop I. Analysis of assisting and opposing flows of the Eyring-Powell fluid on the wall jet nanoparticles with significant impacts of irregular heat source/sink. Case Stud Therm Eng 2023;49:103209.

 [Crossref]
- [26] Ali MM, Akhter R, Alim MA. MHD natural convection and entropy generation in a grooved enclosure filled with nanofluid using two-component non-homogeneous model. SN Appl Sci 2020;2:571. [Crossref]
- [27] Ali MM, Alim MA, Akhter R, Ahmed SS. MHD natural convection flow of CuO/water nanofluid in a differentially heated hexagonal enclosure with a tilted square block. Int J Appl Comput Math 2017;3:1047–1069. [Crossref]
- [28] Ali MM, Akhter R, Alim MA. Performance of flow and heat transfer analysis of mixed convection in Casson fluid filled lid-driven cavity including

- solid obstacle with magnetic impact. SN Appl Sci 2021;3:250. [Crossref]
- [29] Akhter R, Ali MM, Alim MA. Hydromagnetic natural convection heat transfer in a partially heated enclosure filled with porous medium saturated by nanofluid. Int J Appl Comput Math 2019;5:52. [Crossref]
- [30] Akhter R, Ali MM, Alim MA. Entropy generation due to hydromagnetic buoyancy-driven hybrid-nanofluid flow in partially heated porous cavity containing heat conductive obstacle. Alex Eng J 2023;62:17–45. [Crossref]
- [31] Dang K, Makkar V, Sharma N. Numerical analysis of three-dimensional magnetohydrodynamics

- non-Newtonian free stream flow induced by permeable stretching surface. J Therm Eng 2024;10:1465–1479. [Crossref]
- [32] Garvandha M, Gajjela N, Narla V, Kumar D. Thermodynamic entropy of a magnetized nanofluid flow over an inclined stretching cylindrical surface. J Therm Eng 2024;10:1253–1265. [Crossref]
- [33] Shaikh GM, Memon AA, Memon MA, Yashkun U, Obalalu AM, Köten H. Numerical study of flow behavior and heat transfer of ternary water-based nanofluids in the presence of suction/injection, stretching/shrinking sheet. J Therm Eng 2024;10:1021–1043. [Crossref]